JOURNAL OF GEOPHYSICAL RESEARCH, VOL. 113, B02204, doi:10.1029/2007JB005133, 2008

Numerical simulations of volcanic jets: Importance of vent overpressure

Darcy E. Ogden,[1] Kenneth H. Wohletz,[2] Gary A. Glatzmaier,[1] and Emily E. Brodsky[1]

Received 24 April 2007; revised 5 October 2007; accepted 5 November 2007; published 29 February 2008.

[1] Explosive volcanic eruption columns are generally subdivided into a gas-thrust region and a convection-dominated plume. Where vents have greater than atmospheric pressure, the gas-thrust region is overpressured and develops a jet-like structure of standing shock waves. Using a pseudogas approximation for a mixture of tephra and gas, we numerically simulate the effects of shock waves on the gas-thrust region. These simulations are of free-jet decompression of a steady state high-pressure vent in the absence of gravity or a crater. Our results show that the strength and position of standing shock waves are strongly dependent on the vent pressure and vent radius. These factors control the gas-thrust region's dimensions and the character of vertical heat flux into the convective plume. With increased overpressure, the gas-thrust region becomes wider and develops an outer sheath in which the erupted mixture moves at higher speeds than it does near the column center. The radius of this sheath is linearly dependent on the vent radius and the square root of the overpressure. The sheath structure results in an annular vertical heat flux profile at the base of the convective plume, which is in stark contrast to the generally applied Gaussian or top-hat profile. We show that the magnitude of expansion is larger than that predicted from previous 1D analyses, resulting in much slower average vertical velocities after expansion. These new relationships between vent pressure and plume expansion may be used with observations of plume diameter to constrain the pressure at the vent.

Citation: Ogden, D. E., K. H. Wohletz, G. A. Glatzmaier, and E. E. Brodsky (2008), Numerical simulations of volcanic jets: Importance of vent overpressure, *J. Geophys. Res.*, *113*, B02204, doi:10.1029/2007JB005133.

1. Introduction

[2] In large, explosive volcanic eruptions, the eruptive fluid issues from the vent as a high speed, compressible gas with entrained solid particulates. It is important to quantify the behavior of this gas-thrust region because it provides a connection between the fluid dynamics in the conduit and that of the buoyant column. If the eruptive fluid velocity is at or greater than sonic and vent pressure is higher than atmospheric pressure, the dynamics will be complicated by the presence of standing shock waves that can drastically alter the distribution of the vertical heat flux necessary for eruption column stability. The fluid dynamics and structure of a compressible jet issuing from a sonic nozzle into an ambient atmosphere of lower pressure are well known from experimental, analytical and computational studies [e.g., *Crist et al.*, 1966; *Young*, 1975; *Norman et al.*, 1982; Figure 1]. Although application of compressible jet dynamics to explosive volcanic eruptions was first suggested over 25 years ago by *Kieffer* [1981], the concept has yet to be widely applied in modeling and analysis of explosive eruption columns.

[3] In this paper, we present computational results that quantify the important effects of vent pressure on the fluid dynamics of volcanic jets and show that overpressured jets produce vertical heat flux profiles that are drastically different than those of pressure-balanced jets. (Note: to avoid confusion, here we use the physics convention and consider "heat flux" the thermal energy transfer per area per unit time (J m^{-2} s^{-1}) and "heat flow" the thermal energy transfer integrated over an entire area per time (J s^{-1}). In volcanology literature, the term "heat flux" is often used to mean either of these things [e.g., *Woods*, 1988; *Mastin*, 2007]). The simulations shown here are time-dependent, though they assume a steady vent condition. Through these simulations, we quantify the effects of vent pressure and radius on plume radius and heat flux distribution after expansion of the jet. This may allow the prediction of major features of the eruptive structure. We do not consider the effects of variations in conduit dynamics, buoyancy, or the presence of a crater in order to focus only on the effects of vent pressure and radius alone. This study is not a complete picture of the complicated flow dynamics of a volcanic eruption. Rather, the results presented here could be considered the "simplest case" to which one could compare the dynamics resulting from more complicated simulations and observations of high-pressure volcanic jets.

[1] Earth & Planetary Sciences Department, University of California at Santa Cruz, Santa Cruz, California, USA.
[2] Los Alamos National Laboratory, Los Alamos, New Mexico, USA.

0148-0227/08/2007JB005133$09.00

[4] Although fixing the vent pressure to that of the surrounding atmosphere drastically limits the complexity of the flow field, this simplifying assumption allowed fundamental aspects of volcanic eruption dynamics to be determined. We briefly highlight only a few of them here (for a more thorough review, see *Valentine* [1998] and *Woods* [1998]).

[5] *Wilson et al.* [1978] demonstrate that eruptive columns behave like convective thermal plumes [*Morton et al.*, 1956] with a height proportional to the quarter-root of mass flow. This important finding built upon the earlier prediction that eruptive mass flow is determined by conduit and vent shape and size [*Wilson*, 1976]. Since that time, 30 years of observation and experiments have supported Wilson's predictions and demonstrated that vent shape and size also evolve during the course of an eruption [*Wohletz et al.*, 1984; *Woods*, 1995; *Valentine and Groves*, 1996; *Sparks et al.*, 1997b]. Notably in the last decade, a research group now at the Instituto Nazionale di Geophysica e Volcanologia of Pisa demonstrated the advantages of making nonlinear numerical simulations in two and three dimensions with sophisticated constitutive relationships and subgrid-scale turbulence parameterizations [e.g., *Dobran*, 1992; *Macedonio et al.*, 1994; *Papale et al.*, 1998; *Neri et al.*, 2007]. These models have improved our understanding of the factors that influence eruptions including magma viscosity, rheology and composition.

[6] Kieffer first suggested that the well-understood fluid dynamics of an overpressured, supersonic jet could describe volcanic eruption dynamics; she used this understanding to explain the lateral blast of Mount St. Helens on May 18, 1980 [*Kieffer*, 1981]. She applied the method of characteristics to solve for the general flow field and locations of standing shock structures in the proximal areas of the blast (for a description of this commonly used method, see [*Thompson*, 1972]). This approach was later expanded [*Kieffer*, 1989] and used with laboratory experiments of overpressured jets as volcanic analogs [*Kieffer and Sturtevant*, 1984]. This theory of volcanic jets has been more widely applied in the planetary volcanism regime, e.g., sulfuric plumes on Io [*Kieffer*, 1982], where large overpressure ratios are more easily achieved due to low atmospheric densities. However, the theory that the gas-thrust region of volcanic jets may controlled by compressibility effects (and associated shock waves) has not been widely applied to eruption columns on Earth in most studies. These effects are typically assumed to be ''small'' and to have little influence on the dynamics of the larger column [e.g., *Woods*, 1988].

[7] Groups at Los Alamos National Laboratory and the Instituto Nazionale di Geophysica e Volcanologia of Pisa have performed a number of simulations including the effects of compressibility and vent pressure. *Wohletz et al.* [1984] applied an implicit multifield Eulerian numerical method to simulate the initial phases of a large caldera-eruption, showing that overpressure produces a blast wave analogous to the physics of a shock tube. Later, *Valentine and Wohletz* [1989] computed later-stage eruption column development, finding that overpressure is a dominant control of whether or not column collapse occurs. Using computational simulations, *Neri et al.* [1998] and *Neri et al.* [2002] show that overpressured, supersonic volcanic jets accelerate vertically and expand laterally much more rapidly than jets issuing at atmospheric pressure resulting in a more complicated fluid dynamics. Most recently, *Pelanti* [2005] developed a numerical algorithm for modeling of high speed, compressible multiphase flows. Her simulations of overpressured jets demonstrate the importance of accounting for shocks in the gas-thrust region. *Woods and Bower* [1995] also explore the effects of rapid expansion and decompression from shock waves in one-dimensional (1D) semi-analytical conduit and plume models with and without a crater. The results of our study are compared to previous work in the discussion section.

[8] Although not extensively studied in volcanology, numerous experimental, analytical and computational studies on overpressured supersonic jets at laboratory and machine scale have yielded a wealth of information about this complicated and often counterintuitive fluid dynamics. With the development of rocketry and high-speed air travel in the mid-20th century, laboratory experiments of supersonic jets [e.g., *Ladenburg et al.*, 1949] emerged. These experiments consist of gas at high pressure expanding through a nozzle, accelerating to sonic or supersonic velocities, and exiting into a quiescent chamber (or atmosphere) at lower pressure. A jet is considered underexpanded if the pressure at the end of the nozzle (i.e., beginning of the atmosphere) has not fully dropped to the atmospheric pressure. In other words, the ratio (K) of the pressure at the vent (P_{vent}) to the pressure in the atmosphere (P_{atm}) is greater than one. Similarly, jets are considered overexpanded and perfectly expanded when $K < 1$ and $K = 1$, respectively. Here we use the term ''overpressured'' to refer only to the higher pressure at the vent relative to that of the undisturbed atmosphere. Counterintuitively, expansion of overpressured gas chambers through vents can result in values of P_{vent} that are underpressured or overpressured relative to P_{atm} or equal to P_{atm} depending on the shape of the vent. In volcanic eruptions, this is particularly important since most eruptions take place through a vent or crater. Some straight-sided vents may decompress a fluid without the formation of shock waves [*Woods and Bower*, 1995; *Pelanti*, 2005]. However, the reality of vent shape is much more complicated as its evolution is coupled to the flow. Although not included in this study, the effects of vent shape likely represent a first order control of eruption dynamics that needs to be addressed.

[9] Various imaging techniques, including, shadowgrams, Schlieren photographs, and interferograms have been used to document density variations and flow field structure within experimental jets. The early experimental studies [e.g., *Ladenburg et al.*, 1949; *Lewis and Carlson*, 1964; *Crist et al.*, 1966; *Antsupov*, 1974; *Chang and Chow*, 1974] provided information about the general flow field (Figure 1) and empirically determined relationships between the dimensions of the standing shock structures and the vent radius (r_{vent}), the Mach number (M_{vent}) at the vent (i.e., the ratio of the fluid velocity, v, to the sound speed, c), the overpressure ratio (K) and the isentropic expansion coefficient (i.e., the ratio of specific heats, γ) of the gas.

[10] These empirical relationships determined by the experimental studies suggest a 1D analytical solution for Mach disk height, prompting a number of analytical studies of underexpanded jet dynamics [e.g., *Adamson and Nicholls*, 1959; *Young*, 1975; *Ewan and Moodie*, 1986]. Using first

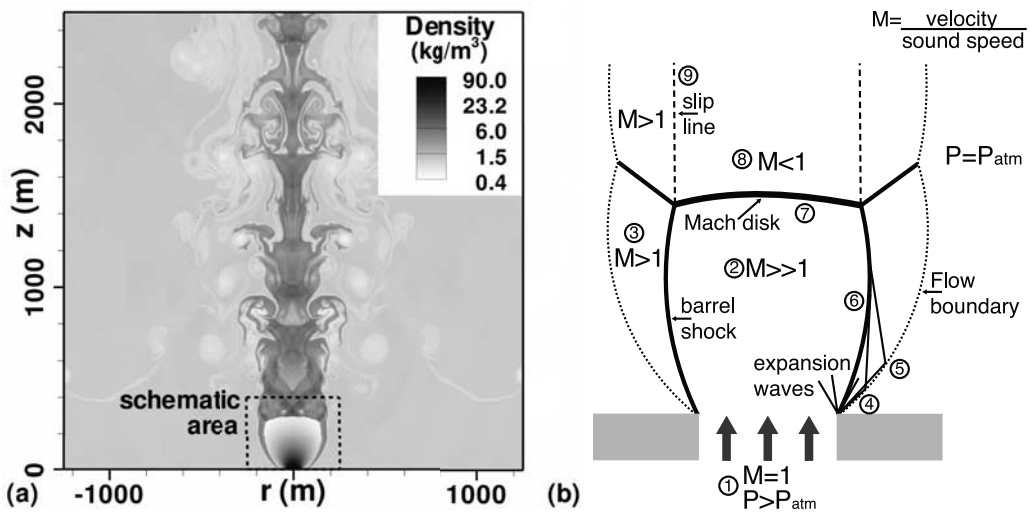

Figure 1. A snapshot of a simulated underexpanded jet (a) with a schematic describing the flow field at the base (b). As fluid flows from a nozzle at sonic velocities with a pressure that is greater than the atmospheric pressure (1), the fluid undergoes Prandtl-Meyer expansion, rapidly accelerating to high Mach numbers (2, 3) and decreasing in pressure and density. A continuous series of expansion waves form at the nozzle exit (4), which are reflected as compression waves from the free surface at the jet flow boundary (5). These compression waves coalesce to form a barrel shock (6) roughly parallel to the flow, and a standing shock wave called a Mach disk (7) perpendicular to the flow. The high Mach number fluid crossing the Mach disk undergoes an abrupt decrease in velocity to subsonic speeds (8), and increases in pressure and density. The resulting fluid dynamics after the Mach disk consist of a slow moving (subsonic) core surrounded by a fast moving (supersonic) shell with a turbulent eddy producing shear layer, or slip line (9), dividing these regions. The length scales of this structure are dependent on the nozzle diameter and the ratio of the inflow pressure to the ambient pressure and are weakly dependent on the isentropic expansion coefficient of the fluid.

principles and some assumptions of ideal behavior, these studies verified that, for a given mass flux at the vent, the Mach disk height is proportional to the vent radius and the square root of the overpressure (as well as a limited dependence on γ). In addition to these 1D solutions, semi-analytical solutions using the method of characteristics [e.g., *Chang and Chow*, 1974] have also provided information about the location and strength of shock waves in underexpanded jets. These methods compare well to experimental jets in the region up to and including the Mach disk.

[11] Both experimental and analytical studies of underexpanded jets have provided insight to the basic fluid dynamics in this regime. However, each is limited in scope. The measurements in experimental studies are strongly limited by the magnitude of velocities, the presence of shock waves and temporal and spatial resolution. Analytical studies can be very applicable to the flow field just downstream of the vent. However, after the first Mach disk, the flow field typically becomes too turbulent for the method of characteristics [*Thompson*, 1972]; and the lack of correlation between fluid velocities of the axial and outer regions precludes a 1D treatment downstream of the first Mach disk [*Chang and Chow*, 1974].

[12] The limitations of analytical solutions and experimental design and measurement lead to the development of computational studies of the flow dynamics of underexpanded jets [e.g., *Norman et al.*, 1982; *Gribben et al.*, 2000; *Ouellette and Hill*, 2000; *Li et al.*, 2004; *Cheng and Lee*, 2005]. Unlike laboratory experiments, computational simulations provide spatial and temporal information about the fluid flow limited only by computational power, not instrument capabilities. In addition, computational simulations do not require the simplifying approximations needed for analytical methods. These advantages enable computational studies to focus on the more complicated aspects of the fluid dynamics, like the axial flow profile downstream of the Mach disk and the turbulent entrainment and mixing of particle laden jets [e.g., *Post et al.*, 2000]. Of course, computational studies also have limitations, which we describe in the discussion section.

2. Methods

[13] Thirty-five time-dependent simulations of pseudogas jets expanding into ambient air were produced for a range of vent radii and overpressure ratios. These simulations are performed in the absence of gravity in order to isolate the effects of compressibility. (Simulations of volcanic jets with gravity and a stratified atmosphere are presented by *Ogden et al.* [2008]). The simulations for this study were performed with CFDLib, a computational fluid dynamics library developed at Los Alamos National Laboratory. CFDLib utilizes a finite volume computational scheme with cell-centered state variables to solve the Navier-Stokes equations for multiple fluids [*Kashiwa and VanderHeyden*, 2000]. It is written in modular format and can solve a variety of computational fluid dynamics problems in one-, two-, or three-dimensions. It utilizes a multiblock data structure that is highly efficient when run on parallel processing supercomputers. For compressible materials, CFDLib uses a

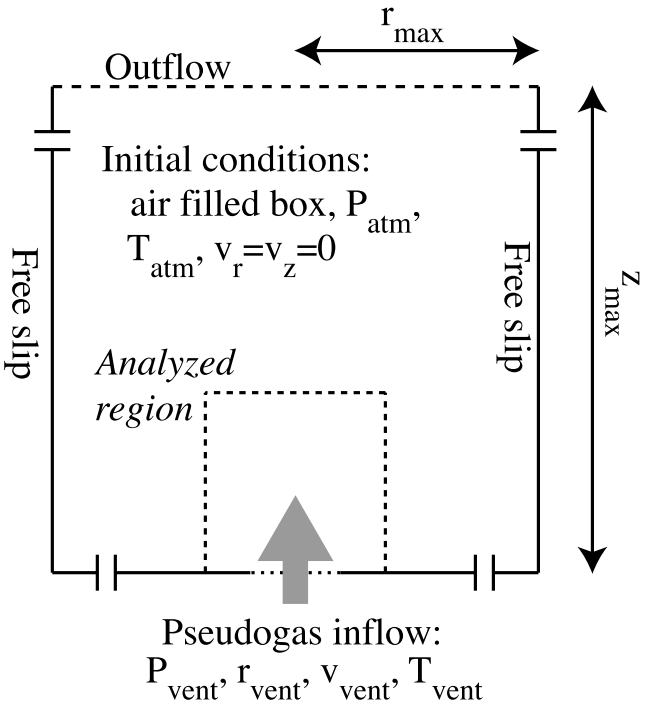

Figure 2. Simulation design. Thirty-five time dependent simulations of overpressured volcanic jets were run with CFDLib in a 2D cylindrical mesh with an axis of symmetry passing through the jet centerline. We begin with a cylinder of air at rest and specify an outflow condition at the top of the box, a small inflow boundary representing the vent at the base, and free-slip boundaries everywhere else. An inflow of pseudogas at sonic speeds is specified at the base. The simulations consist of seven different overpressure values at the vent (K = 1, 5, 10, 20, 40, 80, and 100), and five different vent radii (r_{vent} = 10, 20, 40, 80, and 100 m). The height (z_{max}) and width (r_{max}) of the mesh are about ten and five times the expected height of the first Mach disk, respectively. We present data from the small subsection of the total mesh, the "analyzed region", in the remainder of this paper.

variation of the Implicit Continuous-fluid Eulerian (ICE) method, developed in the late 1960s [*Amsden and Harlow*, 1968; *Harlow and Amsden*, 1975].

[14] Modeling supersonic turbulent flow requires a numerical technique that can resolve shock waves with high precision. CFDLib employs a modified Godunov method [*Godunov*, 1999], well established as one of the best methods for this type of problem, which can resolve a shock front with a small number of grid cells. The simulations we present here were performed using a cylindrically symmetric two-dimensional (2D) mesh of an air filled cylinder initially at rest with a pressure (P_{atm}) and temperature (T_{atm}) of 101,325 Pa and 298 K, respectively (Figure 2). In the middle of the cylinder at the bottom we specify an inflow boundary to simulate a volcanic vent. The top of the cylinder allows outflow of heat and fluid. The side and bottom boundaries (excluding the vent) are impermeable, stress-free boundaries. We stop our simulations when the eruptive fluid reaches the top of the cylinder, which takes between 3 and 125 s, depending on the case simulated. These simulations typically require from 15,000 to 200,000 numerical time steps.

[15] In order to minimize complexity and present our results in context of previous efforts, we model the eruptive fluid as a pseudogas and the atmosphere as a simple diatomic gas, both behaving as ideal gases. The pseudogas approximation treats the entrained particles as another species of gas, remaining perfectly mixed with a vapor phase (steam) such that the two species coexist in perfect thermodynamic and mechanical equilibrium.

[16] To fully specify the eruptive fluid as an ideal gas mixture, we determine the effective gas constant (R_{fluid}) and the isentropic expansion coefficient (Γ). For the pseudogas approximation, $R_{fluid} = nR_{gas}$, where n is the mass fraction of volatiles in the mixture and R_{gas} is the gas constant for the vapor phase [*Kieffer*, 1981]. We assume a rhyolitic magma composition with 4 wt.% aqueous fluid (R_{gas} = 461.5 J/kgK), a mid-range value for magma volatile content [*Sparks et al.*, 1997a]. Our eruptive fluid then has R_{fluid} of 18.46 J/kgK, that is, a molecular weight of 450.4 kg/kmol. The isentropic expansion coefficient for a pseudogas is defined as

$$\Gamma = \frac{nC_p + (1-n)C_s}{nC_v + (1-n)C_s} \quad (1)$$

where C_p and C_v are the specific heat capacities of the gas (steam) at constant pressure and volume, respectively, and C_s is the specific heat capacity of the entrained (solid) particles. We use C_s = 1000 J/kgK, an average value for volcanic rock. Although C_p and C_v vary with temperature and pressure, the equation is dominated by C_s (since $n \ll 1$). Therefore we choose a fixed Γ of 1.02. Within the range of temperatures and pressures computed in our simulations, this fixed value is always within less than a percent of Γ calculated with the varying C_p and C_v. The physical meaning of this value of Γ is that our pseudogas behaves as an almost perfectly isothermal gas (Γ = 1), which is expected for eruptive fluids in which sufficiently small particles continuously supply heat to the expanding gas [*Kieffer*, 1981].

[17] We assume a choked flow condition at the vent; therefore the inflow velocity is the sound speed of the eruptive fluid, $c = (\Gamma\ R_{fluid}\ T_{vent})^{1/2}$, where T_{vent} is the temperature of the eruptive fluid at the vent. It has been shown analytically [*Young*, 1975] and experimentally [*Wu et al.*, 1999] that shock dimensions in underexpanded jets do not depend on the ratio T_{vent}/T_{atm} below supercritical temperatures. For all of the simulations we present here, we specify a T_{vent} of 1200 K. Therefore the inflow velocity at the vent is the same for all of our simulations, 150.3 m/s. In reality, conduit dynamics leading to vent exit conditions are highly varied and non-linear. We stress that we are not taking into consideration many of the known variations, choosing instead to focus on the effects of vent radius and overpressure on a specific vent exit condition.

[18] We perform simulations using five different vent radii (r_{vent}): 10, 20, 40, 80, and 100 m. For each r_{vent}, we simulate seven different overpressure ratios: K = 1, 5, 10, 20, 40, 80 and 100. We vary the pressure of the eruptive fluid by changing the density of the eruptive mixture

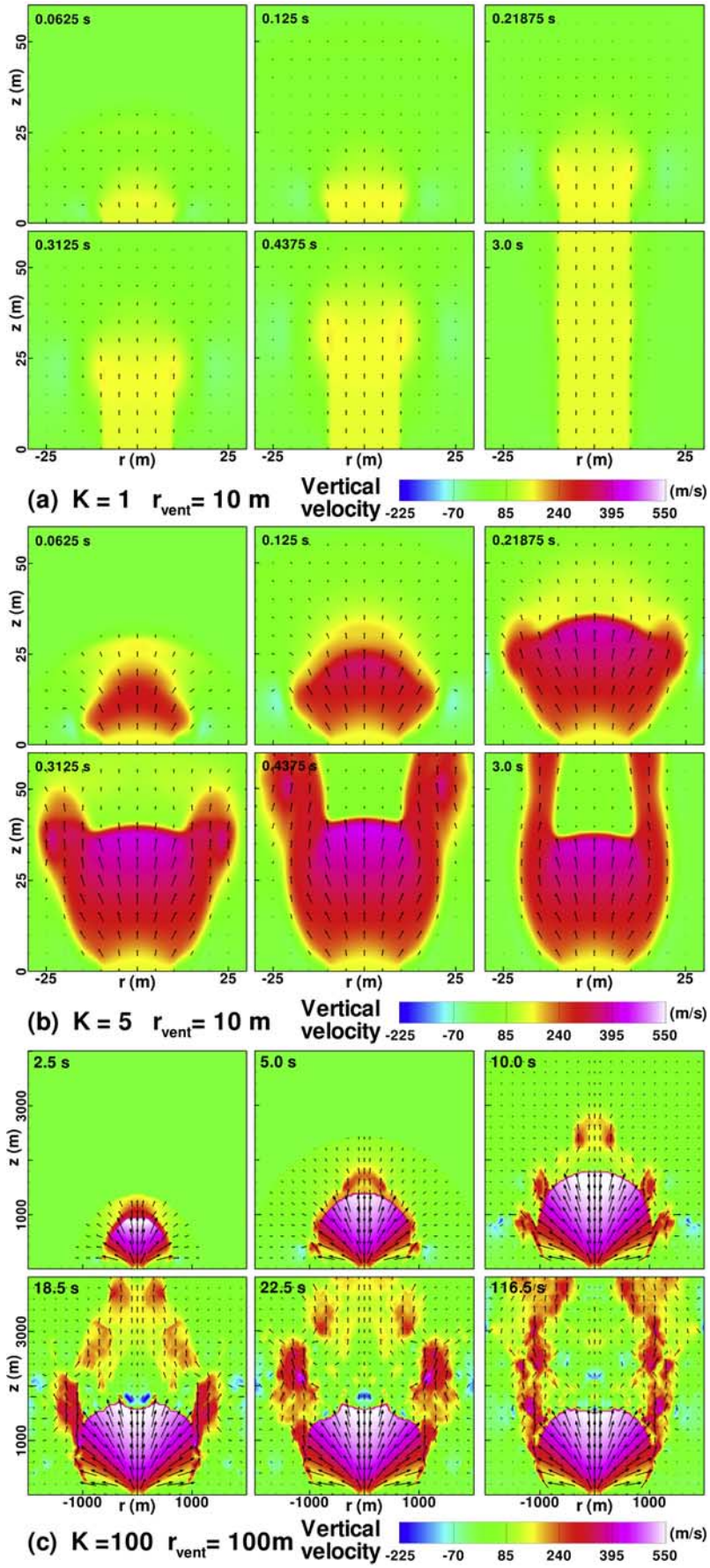
0.0625 s
0.125 s
0.21875 s
0.3125 s
0.4375 s
3.0 s
z (m)
r (m)
(a) K = 1 r_vent= 10 m
Vertical velocity
(m/s)
-225 -70 85 240 395 550
(b) K = 5 r_vent= 10 m
2.5 s
5.0 s
10.0 s
18.5 s
22.5 s
116.5 s
(c) K =100 r_vent= 100m

Figure 3

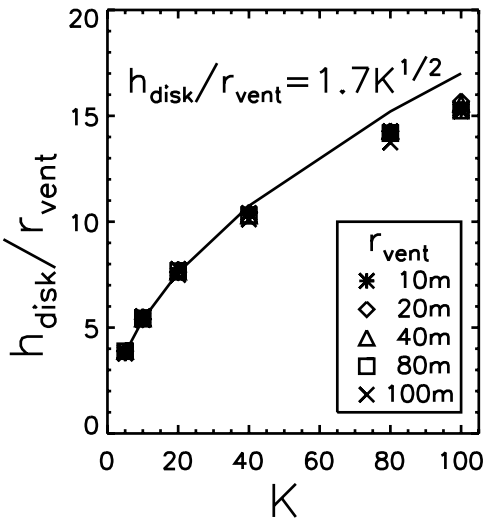

Figure 4. Mach disk height as a function of overpressure for all overpressured simulations. The time averaged Mach disk height on the jet axis normalized to vent radius is shown to be directly dependent on the square root of the overpressure. Symbols are data from simulations. Solid curve is the approximate power law that describes the data. The overprediction at large values of K is likely due to the Mach disk being pushed downward by turbulent eddies produced at high overpressures.

according to an ideal gas equation of state so that the density of the eruptive fluid at the vent (ρ_{vent}) is

$$\rho_{vent} = \frac{KP_{atm}}{R_{fluid}T_{vent}} \quad (2)$$

Using the values given for R_{fluid}, T_{vent} and K, we solve equation (2) for inflow densities ranging from about 4.6 to 460 kg/m^3 for our simulations.

[19] We determine a simulation domain height and diameter (z_{max} and $2r_{max}$ in Figure 2) to be about 10 times the anticipated Mach disk height, estimated with the empirical formula of *Lewis and Carlson* [1964]. This consideration places the boundaries far enough away so they do not affect the results of the simulations. We use a uniform mesh with a cell size based on the simulation height. For simulation heights of 0-2 km, 2-5 km and 5–15 km we use uniform square cells with widths of 1, 2 and 4 m, respectively. We have tested the effects of smaller cell sizes on our simulations and find negligible differences in the flux profiles and jet structures.

[20] Because numerical diffusion is resolution dependent and the jet flow regime is dominated by inertial forces, we further simplified our simulations by specifying zero viscous and thermal diffusivities. For these experiments, it is easy to show that their characteristic effects are much smaller than the imposed advection; setting them to typical values for the atmosphere and erupting fluid produced no visible differences, but their specific parameterization is expected to be important for other eruptive flow regimes.

[21] Snapshots (graphical portrayal of the calculated flow field at a specific time) are presented for qualitative understanding of the flow structures. All other plots are time averages of the data from the final 4/5 of each simulation, which consists of the time after the establishment of the steady state barrel shock and Mach disk structures. All data presented for radial profiles are taken from heights 25% higher than the time-averaged height of the Mach disk for each simulation.

3. Results

3.1. General Flow Structure

[22] Our simulations closely match the expected behavior of a supersonic, high-pressure jet as described in Figure 1. An example of the development of this structure can be seen in the series of vertical velocity snapshots in Figure 3b (within the "Analyzed region" indicated in Figure 2) for the simulation of K = 5 and r_{vent} = 10 m. All of our simulations begin with a compression wave (bow shock) that precedes the eruptive fluid. As the fluid expands rapidly from the vent, it accelerates and its pressure, density and temperature decrease. A barrel-shaped shock structure develops, topped with a horizontal Mach disk. The fluid in the core of the jet crosses the Mach disk, undergoing an abrupt decrease in velocity and increase in pressure, density and temperature. The fluid to either side of the standing Mach disk does not experience a strong shock, but flows around the Mach disk forming a high speed, turbulent sheath surrounding the slow moving core. Similar velocity profiles are seen in other simulations of overpressured volcanic jets [*Neri et al.*, 1998, 2002; *Eposti Ongaro and Neri*, 1999; *Pelanti*, 2005]. This flow field is typical of all of our overpressured simulations (K > 1). For comparison, Figure 3a shows snapshots of a pressure-balanced jet (K = 1) with the same vent radius as in Figure 3b and at the same time steps using the same color scale. Pressure-balanced jets behave like incompressible fluids and do not rapidly expand at the vent. Instead, a steady velocity profile persists throughout the column that mimics that of the vent. Figure 3c shows the largest jet of this study, r_{vent} = 100 m K = 100, illustrating the increase in turbulence at higher overpressures. The height of the Mach disk (h_{disk}) in all of our overpressured simulations (Figure 4)

Figure 3. Vertical velocity snapshots for pressure balanced (a) and overpressured (b, c) jets. These simulations highlight the difference in velocity profile between a jet erupting at atmospheric pressure (Figure 3a) and one undergoing rapid expansion from a modest overpressure of 5 times atmospheric (Figure 3b) and a large overpressure of 100 times atmospheric (Figure 3c). The simulations shown in Figures 3a and 3b have vent radii of 10 m and are the smallest simulations in this study. The simulation in Figure 3c is the largest jet simulated and has a vent radius of 100 m. Note that the length scale in Figure 3c is about 60 times that of Figures 3a and 3b. The full velocity vectors are included at every 5 grid cells (larger simulations have larger grid cells). The same color and vector length scale is used for all simulations. The area shown is a subsection of the entire mesh just above the vent. These profiles highlight the marked difference in velocity magnitude and profile between the pressure balanced (Figure 3a) and overpressured (Figures 3b, 3c) cases. Comparison of the smallest overpressured case (Figure 3b) to the largest (Figure 3c) reveals a transition to a more turbulent regime.

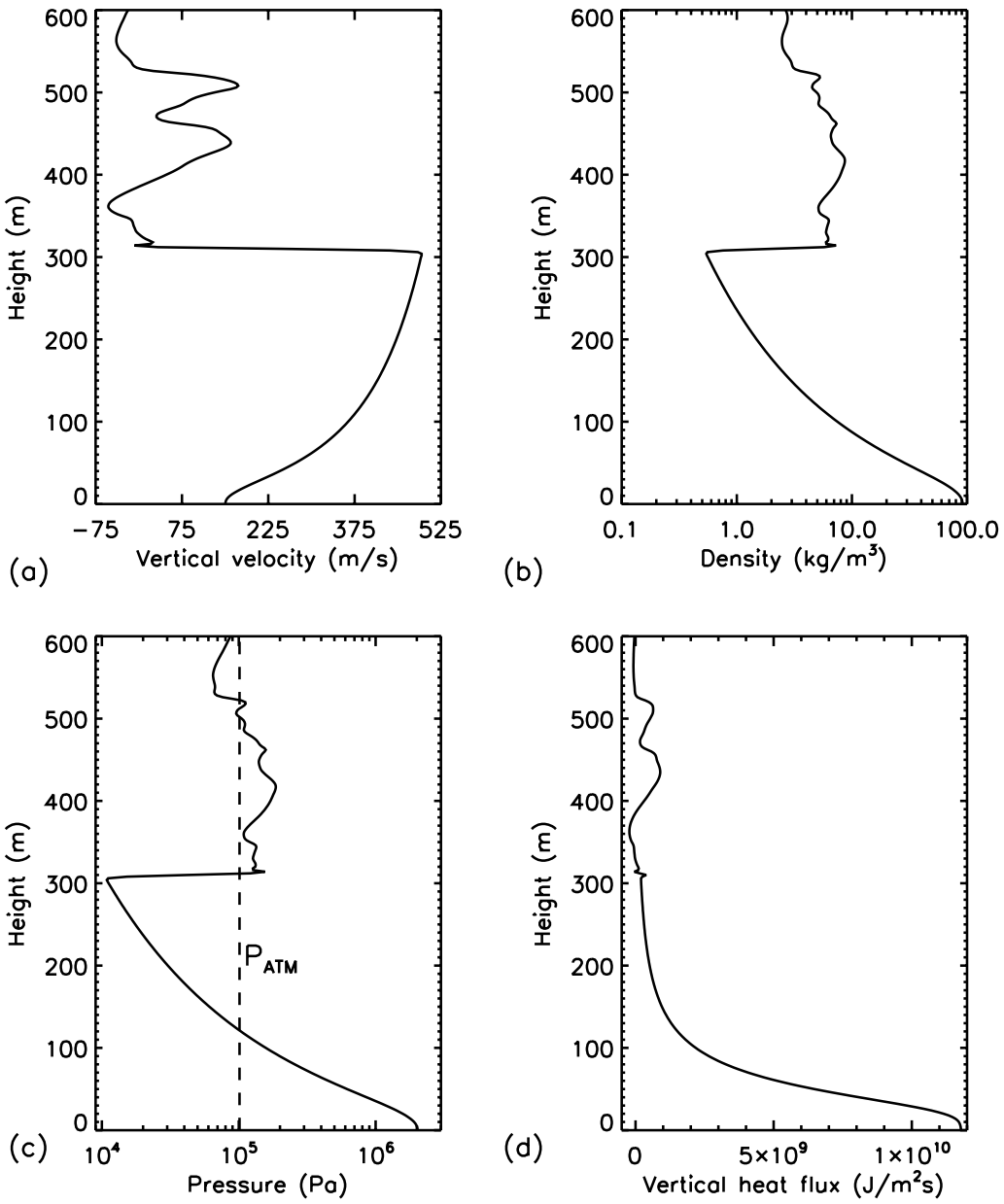

Figure 5. Snapshots of axial profiles of vertical velocity (a), density (b), pressure (c), and vertical heat flux (d) for a typical overpresured simulation. These snapshots from a simulation with r_{vent} = 40 m and K = 20 clearly show the rapid expansion of the gas to pressure values well below atmospheric before returning to approximately atmospheric values after the Mach disk. The stepwise change in vertical velocity and pressure as the fluid crosses the shock wave can be seen in Figures 5a and 5c. These snapshots show only a small portion of the total mesh just above the vent as the mesh extends to 2.5 km.

depends linearly on vent radius (r_{vent}) and on the square root of the overpressure ratio (K): $h_{disk} = 1.7\ r_{vent}\ K^{1/2}$. This is consistent with analytical [*Adamson and Nicholls*, 1959] and experimental results [*Lewis and Carlson*, 1964; *Crist et al.*, 1966; *Antsupov*, 1974; *Addy*, 1981].

3.2. Axial Profiles

[23] Although axial profiles are not adequate to describe the dynamics of the flow field, we include them here to illustrate some of the counterintuitive effects of sonic jet expansion. The effect of the Mach disk on the flow along the jet centerline can be seen in Figure 5, which shows snapshots of axial profiles of vertical velocity (a), density (b), pressure (c) and vertical heat flux (d) for a typical overpressured simulation. The rapid expansion and acceleration of the fluid is clearly seen above the vent, upstream of the Mach disk. In all overpressure cases, the pressure along the axis rapidly decreases, dropping below atmospheric pressure. In our simulations, the pressure just before the first Mach disk ranges from $0.1P_{atm}$ (K = 100 cases) to $0.15P_{atm}$ (K = 5 cases). This overshooting of the expansion to levels below atmospheric pressure during expansion is well known, and its magnitude is dependent on M_{vent}, K, and Γ [e.g., *Adamson and Nicholls*, 1959].

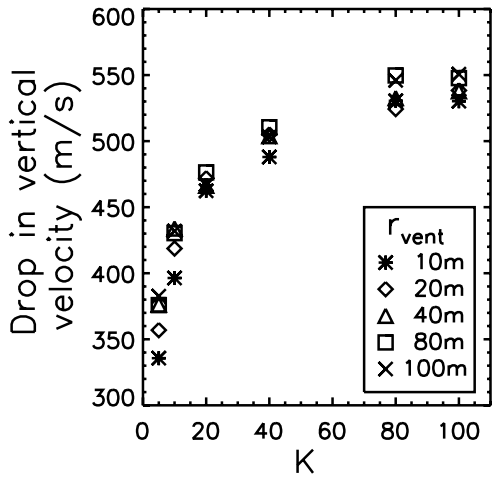

Figure 6. Time-averaged decrease in vertical velocity across the Mach disk on the axis as a function of overpressure for all overpressured simulations. As discussed in the text, increasing overpressure increases axial velocities resulting in stronger Mach disk shocks and a greater decrease in velocity across the shock.

[24] The fluid on the axis continues to accelerate and decompress until it crosses the Mach disk. As the fluid crosses this shock wave, pressure increases in a stepwise manner to something slightly higher than that of the atmosphere for our eruption-scale jet simulations. At this point, the vertical velocity of the fluid on the axis decreases to subsonic speeds. Along the axis, the temperature and density of the fluid decrease rapidly with expansion and increase in an abrupt manner across the Mach disk. The axial vertical heat flux profile below the Mach disk is dominated by the rapidly decreasing density and temperature, decreasing in magnitude with height despite the increase in velocity during the initial expansion.

[25] As the fluid rapidly expands, it undergoes a large acceleration, which is dependent on v_{vent} (sonic in all of the cases presented here), K (a varied parameter), and Γ (1.02 in all cases). Larger initial overpressure ratios (K) cause greater expansion and acceleration of the fluid. This may seem to imply that larger overpressures result in larger vertical velocity on the axis at the base of the buoyant plume. However, due to the Mach disk, the opposite occurs. The higher the Mach number of any compressible fluid before passing through a shock, the stronger the shock will be. That is, the more supersonic the upstreamflow the more subsonic the flow is downstream of the Mach disk. For a perfect gas, this relationship is governed by

$$M_2^2 = \frac{2 + (\Gamma - 1)M_1^2}{2\Gamma M_1^2 - (\Gamma - 1)} \tag{3}$$

where M_1 and M_2 are the Mach numbers upstream and downstream, respectively, of a compressive shock front [*Liepmann and Roshko*, 1957]. Therefore although counterintuitive, an increase in overpressure results in a decrease in fluid velocity on the axis above the Mach disk for the sonic vent conditions we have prescribed. The drop in vertical velocity across the Mach disk as a function of overpressure can be seen in Figure 6.

3.3. Vertical Heat Flux Distribution

[26] The shock structure that develops and the resulting downstream velocity pattern determine the heat and mass flux distributions in the lower part of the plume. Figure 7 shows snapshots of different variables at the same times in the jet region for a typical simulation. The vertical mass flux, ρv_z (Figure 7a), and the vertical advective heat flux, $q = C_p(T_{fluid} - T_{atm})\rho v_z$ (Figure 7b), are dominated by the density (Figure 7c) and fluid temperature (Figure 7d) below the Mach disk and by the vertical velocity (Figure 7e) above the Mach disk. The velocity distribution created by the standing shock structures results in an annular vertical heat flux profile above the Mach disk, i.e., a slowly rising fluid in the core with little advective vertical heat flux surrounded by rapidly rising fluid in a sheath that contains the bulk of the heat flow. A three-dimensional representation of this annular structure is shown in Figure 8b for the case with K = 5 and r_{vent} = 10 m. For comparison, the vertical heat flux profile at the same height for the jet with K = 1 with the same vent radius is shown in Figure 8a. The distinct top-hat vertical heat flux profile is clearly apparent in the pressure-balanced case (Figure 8a), but is replaced by an annular structure in the ovepressured jet with a minimum vertical heat flux on the axis (Figure 8b).

[27] The shape and size of these annular structures depend on the vent radius and the overpressure ratio. Figure 9 shows the vertical heat flux profile in radius for a slice just above the Mach disk for all of our cases. The vertical heat flux profiles in radius above the Mach disk for a given overpressure have the same basic shape and magnitude when normalized to vent radius. Increasing vent radius and increasing overpressure forms wider jets with thicker fast moving sheaths.

[28] The radius of the annulus increases linearly with vent radius and with the square root of the overpressure. Figure 10 shows the radius of the peak vertical heat flux (r_{peak}) above the Mach disk as a function of the overpressure. Our simulations suggest that, to first order, r_{peak} goes as

$$r_{peak} = r_{vent}K^{1/2}. \tag{4}$$

This analytical equation and others presented here are descriptions of data trends and are not best fit calculations. The radius of the Mach disk, which is controlled by the same dynamics that forms the annulus, follows this same general relationship in our simulations and in other experimental and analytical studies [e.g., *Crist et al.*, 1966; *Antsupov*, 1974; *Addy*, 1981; *Cumber et al.*, 1995].

[29] The magnitude of the vertical heat flux in this annular profile drops off with increasing overpressure. Figure 11 shows the peak vertical heat flux (q_{peak}) in the sheath above the Mach disk as a function of overpressure for all overpressured cases. From these data, the magnitude of the vertical heat flux as a function of the vent vertical heat flux (q_{vent}) and overpressure (K) can be estimated as

$$q_{peak} = 3q_{vent}K^{-5/4}. \tag{5}$$

Since q_{vent} increases linearly with K, the difference between the commonly used parameter q_{vent} and the more physically relevant q_{peak} increases with K.

[30] As seen in Figure 9, the width, or thickness, of the fast moving sheath is also a function of vent radius and

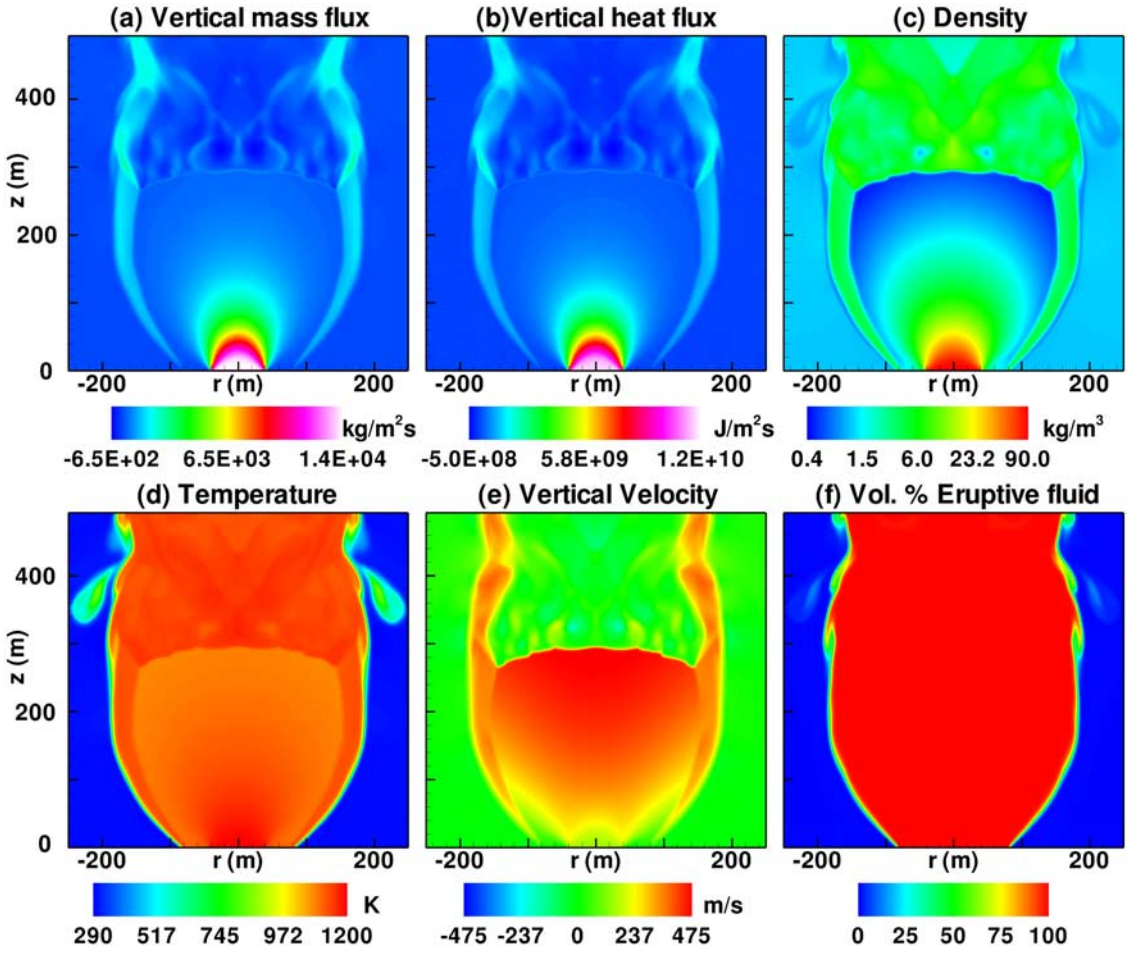

Figure 7. Snapshots of vertical mass flux (a), vertical heat flux (b), density (c), temperature (d), vertical velocity (e), and volume fraction eruptive fluid (f) for a typical overpressured simulation. The vertical velocity profile clearly has a larger influence on the vertical heat flux profile above the Mach disk than the temperature, density, or fluid distribution. The turbulent nature of the simulations can also be seen. Snapshots are of area of interest at t = 20 s for the jet with r_{vent} = 40 m and K = 20.

overpressure. An approximation for this width can be made by simple geometric arguments and by conserving heat flow (Figure 12). A good approximation for the heat flow through the entire sheath (Q, Js^{-1}) is

$$Q = 2\pi r_{peak} q_{peak} w \tag{6}$$

where w is an estimate for the thickness of the ring where $q = \frac{1}{2}\, q_{peak}$. Since the bulk of the heat flow-passes through the sheath and these simulations are relatively steady in time (i.e., heat flow is conserved vertically), a good assumption is that Q can be set equal to the heat flow at the vent (Q_{vent}):

$$Q_{vent} = \pi r_{vent}^2 q_{vent}. \tag{7}$$

Setting equation (6) equal to equation (7), using the empirical relationships shown in equations (4) and (5), and solving for w, we find

$$w = \tfrac{1}{6} r_{vent} K^{3/4}. \tag{8}$$

Thus together, equations (4), (5) and (8) provide a first order description of the vertical heat flux distribution and magnitude above the Mach disk as a function of the radius, overpressure and vertical heat flux at the vent. Alternatively, one could define an annulus with an average heat flux of $\frac{1}{2}\, q_{peak}$, which would have a thickness of $\frac{1}{3} r_{vent} K^{3/4}$.

[31] These crude approximations do not perfectly describe the system. For example, our approximation for r_{peak} (equation (5)) is more accurate at high K and that for w is more accurate at low K (equation (6)). Additionally, how high into the column above the Mach disk this vertical heat flux distribution persists cannot be calculated from these preliminary simulations since buoyancy forces have not been included.

3.4. Mach Disk Stability

[32] In addition to increasing the plume width, an increase in overpressure or vent radius decreases the stability of the Mach disk. Figure 13 shows the variability (in time) of the Mach disk height as a function of the average Mach disk height, h_{disk}, on the axis. At higher overpressures and larger vent radii (i.e., higher and wider Mach disks), the Mach disk height is more time-dependent, and its shape is more undulatory. A fit to the data in Figure 13 gives the standard deviation (σ_h) of the Mach disk height to be proportional to $h_{disk}^{5/4}$.

[33] In general, the larger jets are more chaotic and produce more turbulent eddies than the smaller jets. These turbulent eddies cause more oscillation and disruption as

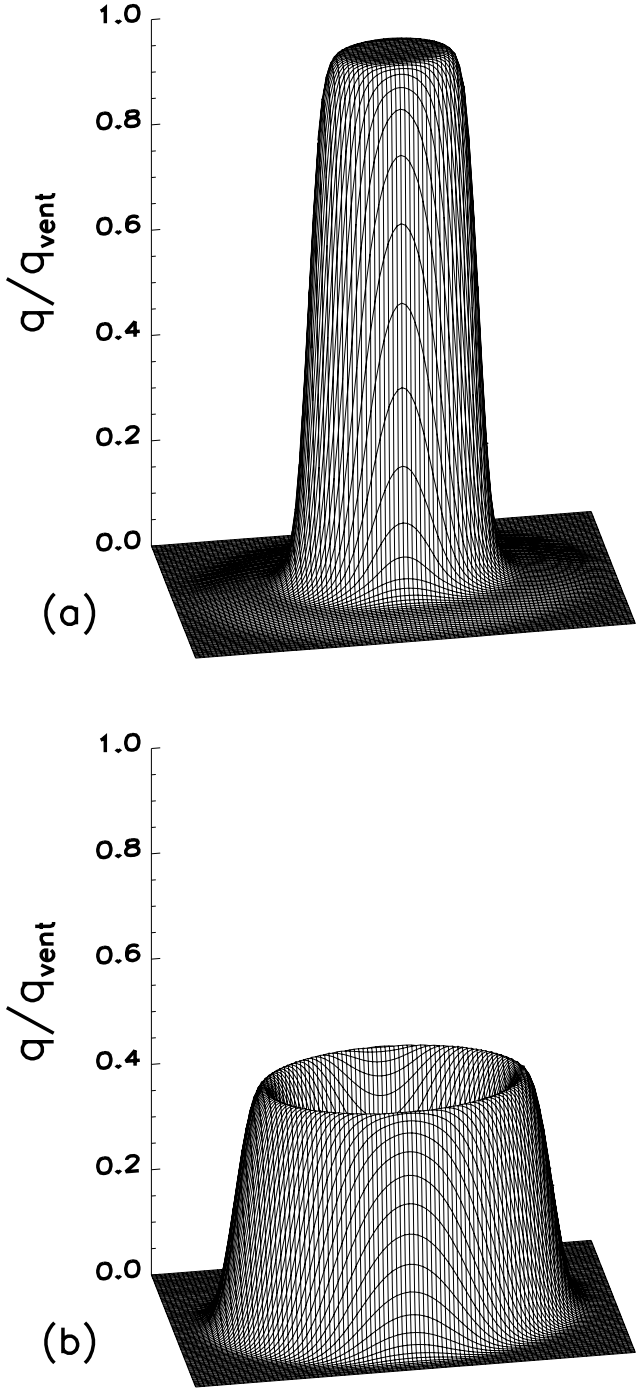

Figure 8. 3D visualization of time-averaged top hat (a) and annular (b) vertical heat flux profiles above the Mach disk rotated about the *z axis*. x- and y-axes are horizontal spatial axes extrapolated from radial profile. Shading and grid scale are the same for both simulations. Figure 8a, a top-hat profile vertical heat flux profile of simulation r_{vent} = 10 m and K = 1, is the expected profile for K = 1 or incompressible fluids. Figure 8b, an annular vertical heat flux profile of simulation r_{vent} = 10 m and K = 5, is typical of all simulations with K > 1. Note the hollow center in Figure 8b and flat top of Figure 8a. The heat flux relative to the vent heat flux in overpressured jets (Figure 8b) is lower than that of pressure balanced jets due to the increased area of the plume.

they interact with the Mach disk. The smaller, more laminar jets have cleaner annular velocity profiles (Figure 9) and smaller turbulent boundary layers, which produce less interference and fewer oscillations in the Mach disk. The interaction between shock fronts and turbulent shear layers is currently a very active area of research as it causes noise known as jet screech in large jet engines.

4. Discussion

4.1. Implications for Plume Models and Hazard Assessment

[34] The majority of volcanic plume analyses used for hazard assessment employ one-dimensional, semi-analytical models that assume the radial distribution of the vertical velocity within the plume to be either a Gaussian or top-hat profile with the highest velocities on the centerline axis. This kind of velocity profile is typically associated with incompressible or pressure-balanced (K = 1) jets and can be seen in Figures 3a and 8a. The velocity profile in a plume controls the magnitude of the air entrainment into the plume and therefore its maximum height and stability. The maximum height of the plume, along with other factors, like rainfall and horizontal wind, determines the direction and extent of the affected fallout region and the amount of long-term atmospheric residence. The amount of entrainment relative to the amount of heat flow also determines the stability of the column and may lead to the formation of dangerous lateral flows by column collapse.

[35] Our simulations of overpressured jets show that within the gas-thrust region, the vertical velocity in a plume develops an annular profile, a fast rising sheath surrounding a much more slowly rising core of the plume. This concentration of mass flux near the boundary of the plume likely changes the entrainment dynamics such that significantly more or less surrounding air is mixed into the plume compared to a plume with the same total heat flow but with the traditional top-hat velocity profile. The effects upon entrainment remain a problem for future study, which also suggests that predictions for column collapse and plume height may also need to be revised. It is uncertain from our simulations whether or not this velocity profile persists into the buoyant region of the plume. At a minimum, the annular velocity profile affects entrainment rates within the gas-thrust region of the jet. This annular profile may persist into the buoyant plume region (especially for large overpressures), therefore affecting the dynamics of the entire column.

[36] It has previously been suggested that the heat flux distribution within the plume may have an important effect on column stability. *Legros et al.* [2000] suggest that the curtain jets present in ring-fissure conduits increase air entrainment making the transition to column collapse more difficult. In our case, the vertical heat flux distribution is controlled by the level of overpressure at the vent, implying a relationship between overpressure magnitude and column height and stability. Preliminary simulations including a stratified atmosphere and gravity are presented by *Ogden et al.* [2008].

4.2. Field Application: Vent Pressure Estimates

[37] The rapid expansion apparent in many volcanic eruptions including the Plinian eruption of Mount St. Helens, 18 May 1980, [*Woods*, 1988], suggest a sonic or

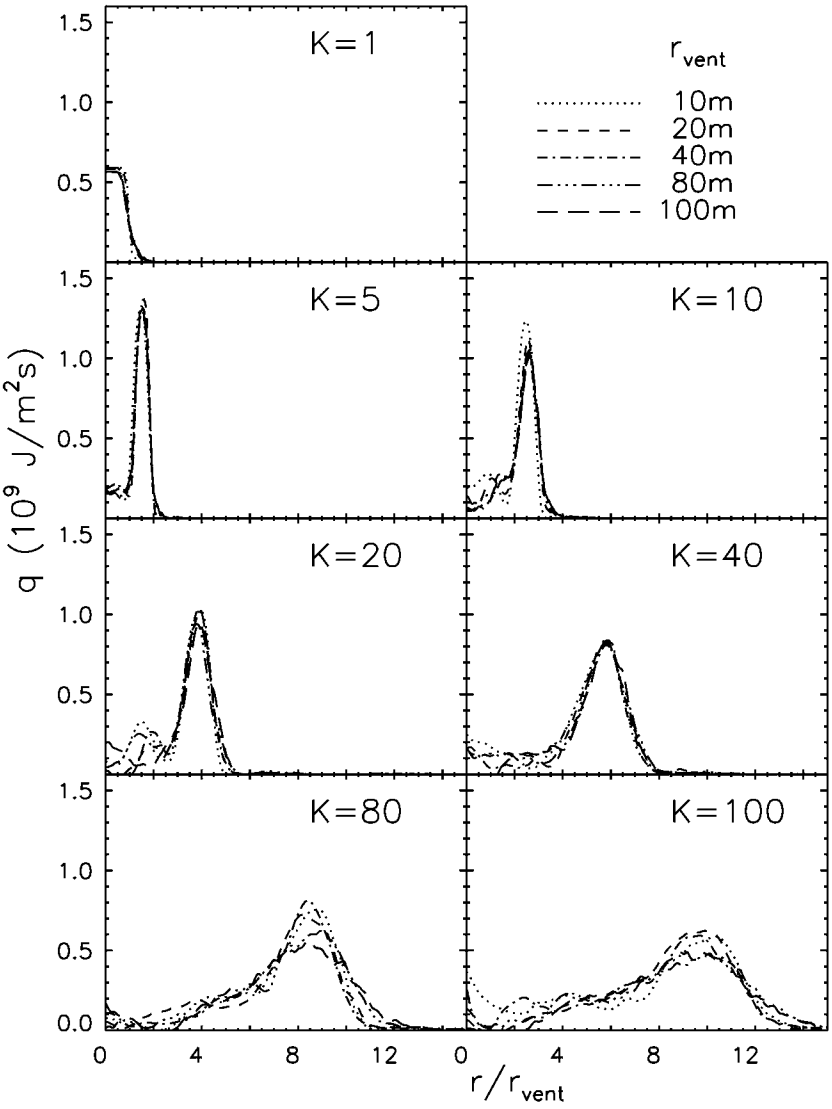

Figure 9. Time-averaged vertical heat flux above the Mach disk as a function of distance from the jet centerline for all simulations. Vertical heat flux (q, Jm^{-2} s^{-1}) above the Mach disk as a function of distance from the jet centerline (r) normalized to the vent radius (r_{vent}). Each frame is a different overpressure value showing the shape of the heat profile as a function of overpressure. The increasing radius of the peak heat flux and the decrease in heat flux with increasing overpressure are shown in Figures 10 and 11, respectively. (Note that the density and therefore the heat flux at the vent increases directly with overpressure. Therefore the apparent increase in heat flux between K = 1 and K = 5 is actually due to the increase in heat flux at the vent.)

supersonic overpressured vent. It may be possible to use the observed plume dimensions to constrain the order of magnitude of this overpressure. Since the fast moving sheath defines the outer part of the plume above the Mach disk, we can use the radius of the peak vertical heat flux in this structure (r_{peak}) as a proxy for plume radius. Equation (4) therefore provides a first-order estimate for vent overpressure based on the ratio of the plume radius in the lower part of the column to the vent radius (r_{vent}). For example, for the Mount St. Helens eruption above, field data suggest r_{vent} = 60 m and $r_{peak} \approx 500$ m [*Woods*, 1988]. Therefore assuming this eruption had a sonic vent velocity, the vent pressure was at least 70 times atmospheric pressure.

[38] Several uncertainties are inherent in this estimation. First, it is based on simulations performed with an ideal gas approximation for a multiphase fluid. Simulations and laboratory experiments with particle-laden jets show that the addition of entrained solid particles makes the barrel shock structure shorter and wider [*Hishida et al.*, 1987; *Dartevelle*, 2006]. Also, the simulations presented here prescribed a Mach number of unity at the vent. Multiphase effects and vent flaring may cause rapidly expanding volcanic eruptions to have higher Mach numbers at the ground surface, which would lead to greater expansion for the same overpressure ratio. The visual plume radius used here (500 m) is actually larger than the radius of the peak velocity in the sheath (r_{peak}) used for this estimate. These

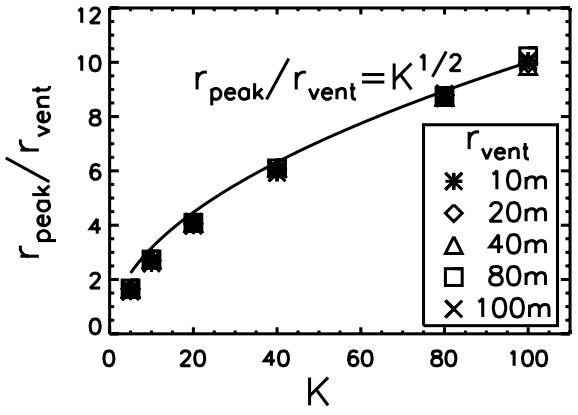

Figure 10. Time-averaged radius of peak vertical heat flux above the Mach disk for all overpressured simulations. The distance of the peak vertical heat flux can be seen as a proxy for plume width in these overpressured jets. The plume width increases linearly with vent radius and the square root of the overpressure. The values plotted here are the radial values under the peaks of the curves in Figure 9. Symbols are simulation data. Line corresponds to only to the equation shown which represents the data trend but is not a calculated curve fit.

considerations suggest that our estimate for the overpressure in the Mount St. Helens eruption may be too large. Volcanic eruptions are also very time-dependent. Our results were obtained by fixing K and r_{vent} and time averaging the plume dimensions. For a real volcanic eruption, K and r_{vent} vary in time. The final measured r_{vent} may be much wider than the r_{vent} that should be associated with the observed r_{peak}, leading to underestimates of overpressure. This analysis also neglects the presence of a crater, which can influence the jet decompression leading to higher Mach numbers at the surface or a different decompression pattern. However, even with these complications, the relationship between plume radius and overpressure ratio (equation 4) provides an order of magnitude estimate for vent overpressure that may help constrain conduit and vent dynamics.

4.3. 1D Analytical Treatments of Overpressured Volcanic Jets

[39] *Woods and Bower* [1995] offer two different treatments of the expansion of eruptive fluid into the atmosphere, one for "free decompression" into the atmosphere and a separate treatment for decompression into a crater. Since our simulations here do not include a crater, we will just consider the former. Additionally, Woods and Bower include the degassing of particulates in their solution. Since this is not included in our models, we remove this complication in the analytical solutions we use for comparison to our models.

[40] In their 1D, analytical model, Woods and Bower apply the momentum principle for a control volume which states that the net force on a fixed volume is equal to the rate of change of momentum within the volume plus the net outflux of momentum through the surfaces. This principle is applicable even in the presence of shock waves and is applied elsewhere to overpressured jets [e.g., *Yüceil and Ötügen*, 2002]. Woods and Bower assume an axisymmetric flow and place the bottom boundary of their control volume across the vent (i.e., our inflow boundary), the side boundaries at the edge of the jet where $P = P_{atm}$, and the top boundary at some height at which $P = P_{atm}$ and the density of the jet is equal to the density of the eruptive fluid at atmospheric pressure. They assume all outflux of vertical momentum takes place through the top and bottom boundaries. They set the vertical force on the bottom and top boundaries equal to the pressure times the area at these locations. The vertical force along the side boundaries is assumed to be only the vertical component of the force from atmospheric pressure along the sloped sides. Geometric arguments show this to be equal to atmospheric pressure times the difference between the areas of the vent and the expanded jet (i.e., the top and bottom boundaries).

[41] This treatment of the side boundary condition results in velocity and area predictions that are not very accurate.

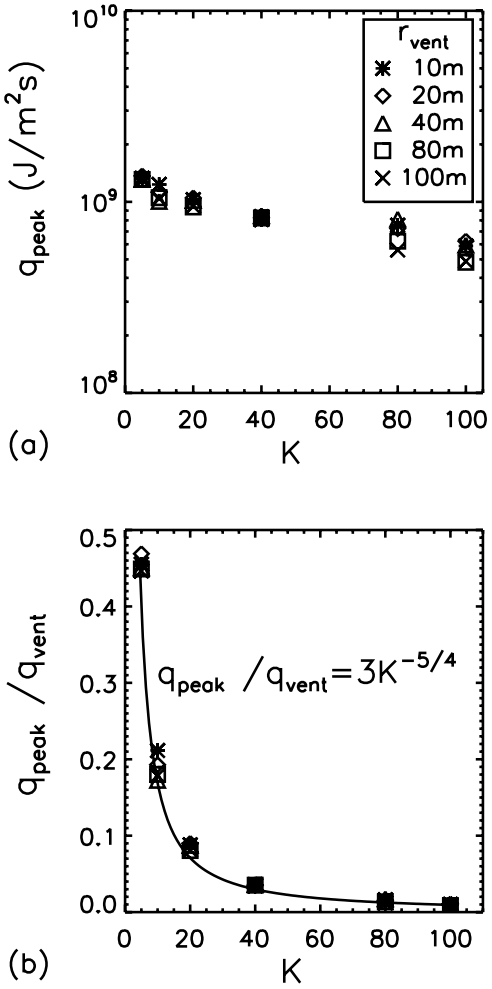

Figure 11. Time-averaged peak vertical heat flux above the Mach disk for all overpressured simulations. (a) The peak vertical heat flux in the plume above the Mach disk is decreased by the overpressure as the greater expansion spreads the jet over a greater area. (b) q_{peak} is normalized to q_{vent} in order to account for the increase in q_{vent} with K. Symbols are simulation data. Line corresponds to only to the equation shown which represents the data trend but is not a calculated curve fit.

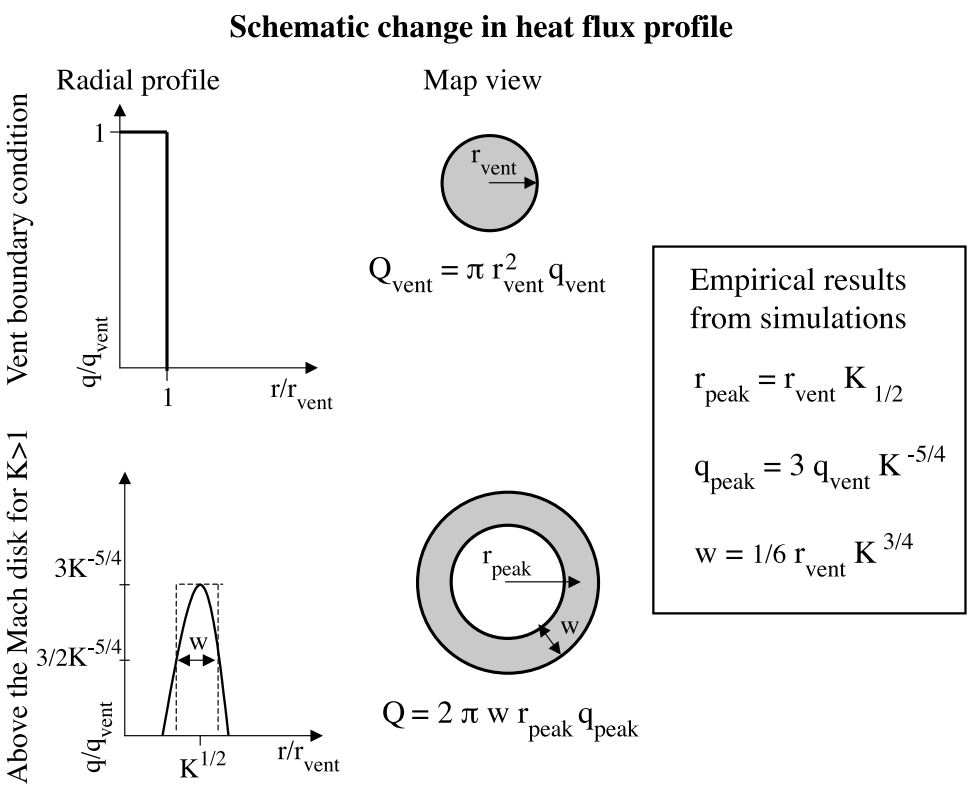

Figure 12. Schematic change in vertical heat flux profile. An illustration showing the geometry of the vertical heat flux distribution at the vent and above the Mach disk. As described in the text, by empirical fit to our data and simple geometric analysis, the shape and magnitude of the vertical heat flux distribution above the Mach disk as a function of overpressure, vent radius, and vent vertical heat flux can be described by the three equations given. Alternatively, one could define an annulus with an average heat flux of $\frac{1}{2}q_{peak}$, which would have a thickness of $\frac{1}{3}r_{vent}K^{3/4}$.

Figure 14 compares the predicted vertical velocities and vent radii from a Woods and Bower type analysis of our vent conditions to the results from our simulations after the fluid has fully expanded. The Woods and Bower type solution for vertical velocity overpredicts the cross-sectionally averaged vertical velocity from our simulations by almost a factor of two (Figure 14a). The plume radius predicted by the Woods and Bower formulation then underpredicts the compositional boundary of the simulated plumes by almost a factor of two (Figure 14b). In fact, the plume radius estimate used in section 4.2 based on the radius of the peak velocity in the sheath ($r_{peak}/r_{vent} = K^{1/2}$) is a better estimate of the plume radius after expansion than is the Woods and Bower analytical prediction.

[42] The simulated values for velocity and plume radius do not match those of the Woods and Bower formulation because the simulations treat the side boundaries much more robustly than is possible in their analysis. There is a significant amount of momentum loss through the side boundaries due to drag and turbulence production that is not taken into consideration in their formulation. This momentum loss results in significantly lower velocities and wider plumes than those predicted by Woods and Bower. Future 1D models of the decompression of volcanic plumes will need to incorporate an appropriate solution for this momentum loss in order to more accurately predict the plume parameters after decompression.

4.4. Laboratory Experiments

[43] Although the linear relationships described in section 3.3 of the shock structures and plume dimensions to vent radius suggest that dimensionality is not important, other features of underexpanded jets downstream of these shocks are not directly dependent on vent radius. Therefore using laboratory experiments of underexpanded jets as volcanic analogs also has its problems. The fluid dynamics of the area downstream of the Mach disk is highly dependent on the turbulence generated at the shear layer between the fast moving sheath and the slow moving core. The magnitude of turbulence is typically estimated by the Reynolds number of the jet, defined as $\mathrm{Re} = UL\nu^{-1}$, where L is a characteristic length scale (e.g., the radius of the jet), U a characteristic velocity, and ν the viscous diffusivity of the eruptive fluid. For our simulations, however, due to numerical viscosity, Re is only about 10^3–10^4, approximately the same order as the laboratory scale simulations of *Kieffer and Sturtevant* [1984]. Estimates for Re for real volcanic eruptions can be greater than 10^{11}[*Kieffer and Sturtevant*, 1984]. Although both our simulations and laboratory experiments have much smaller Reynolds numbers than estimates for real eruptions, both are at least in the turbulent regime for underexpanded

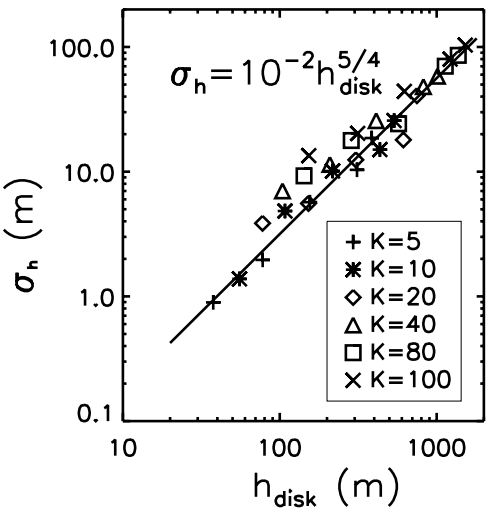

Figure 13. Standard deviation (σ_h) of Mach disk height on the axis as a function of average Mach disk height for all overpressured simulations. Oscillations in Mach disk height are common in overpressured jets and increase with increasing height of the Mach disk. This phenomenon is related to the larger shear layers produced in larger jets and their interaction with the Mach disk. This turbulence production can be quantified by the Reynolds number, which, for these simulations is of the order 10^4. Symbols are simulation data. Line corresponds to only to the equation shown which represents the data trend but is not a calculated curve fit.

jets. For a more complete discussion of the fluid dynamics downstream of the Mach disk, see *Ogden et al.* [2008].

4.5. Overpressured Supersonic Volcanic Jets in Nature

[44] Although the terms "supersonic" and "Mach number" intuitively suggest almost prohibitively large velocities for a real volcanic eruption, they are relatively easy to achieve for even lower energy eruptions due to the effects of mixtures on sound speed. *Kieffer* [1977] shows that the speed of sound in a dusty gas is less than the speed of sound in either the particulates or the gas itself. For eruptive fluids, sound speeds can be as low as tens of meters per second [*Kieffer*, 1977]. Vulcanian, Strombolian, and Plininian eruptions have estimated vent exit velocities ranging from tens to hundreds of meters per second [*Wilson and Self*, 1980], which can easily be sonic or supersonic in particulate laden eruptive fluids. In the simulations presented here, we chose to set the inflow velocity of our eruptive fluid to be exactly sonic in order to perform a parametric study of overpressure. The natural system has much more complexity resulting from conduit dynamics and crater effects that are not included in this study. The interaction between an evolving flaring vent and high-speed multiphase eruptive fluid will be the topic of future work. Although we suspect a range of velocities in nature, our assumption of choked flow provides a minimum vent velocity for overpressured volcanic jets that exhibit these shock structures. With increasing vent velocity, the expansion and shock strength increases, and we would expect more pronounced results. Additionally, it is important to recognize that all current observations of volcanic eruptions only provide estimates of the velocities on the outsides of the eruption column. Laboratory studies of overpressured jets [e.g., *Kieffer and Sturtevant*, 1984] that show the Mach disk structure can only do so because they were able to use optics to average out the turbulent outer flow.

[45] Whether or not an eruption is overpressured, however, is far more complicated. The decompression of a gas through a nozzle or conduit and vent system can result in vent exit pressures that are greater than (K > 1), less than (K < 1), or equal (K = 1) to that of the ambient pressure. This vent exit pressure is dependent on a number of factors, including, but not limited to, the pressure in the magma

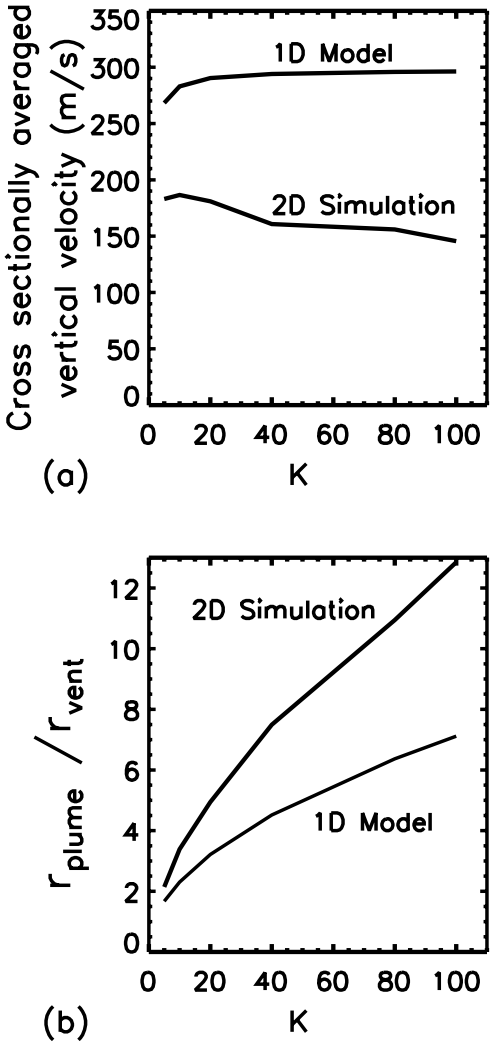

Figure 14. Comparison of simulation output to 1D model. Using the control volume approach of *Woods and Bower* [1995] including simplified jet boundaries, predictions for the vertical velocity (a) and plume radius (b) as a function of jet overpressure are shown (1D Model). For comparison, cross-sectionally averaged velocities (Figure 14a) and plume radii (Figure 14b) of the simulated plumes (2D Simulation) are shown. Likely due to the simplified boundary conditions that do not account for momentum loss and drag along the sides of the jet, Woods and Bower type analytical solutions underpredict the plume radii of an overpressured jets and overpredict their vertical velocities.

chamber, the shape of the conduit and vent, the frictional interaction with the walls, and permeation of gas through the conduit walls. Even without the complicating factors of magma fragmentation, evolution, and rheology, the pressure at the surface can be easily changed by the shape of the vent. One-dimensional analysis shows that simple cone-shaped vents are capable of causing decompression of the eruptive fluid before it reaches the surface [e.g., *Woods and Bower*, 1995], and this process is also demonstrated computationally by *Pelanti* [2005]. In addition, experimental studies have shown that the shape of a jet nozzle plays a role in the shape and size of the barrel shock structure and position of the Mach disk [*Addy*, 1981]. *Kieffer* [1989] suggested that, in explosive eruptions, the flow from sub- to supersonic conditions through the vent can erode the solid host rock into a nozzle shape and size that maximize mass flux. In support of Kieffer's suggestion, preliminary CFDLib simulations of explosive eruptions involving a compressible, multiphase fluid venting through a solid host rock show that the conduit wall rocks do indeed erode to form a nozzle-like vent in response to the stresses imposed by an overpressured jet [*Wohletz et al.*, 2006]. Thus the effects of an evolving vent shape in solid host rock appear to be very important factors in determining the development of eruption columns and our plan is to address this aspect in future work.

4.6. Effects of Simplifications

[46] In addition to holding the vent radius constant in space and time, we make a number of other numerical approximations in order to limit the complexity of the problem and quantify the effects of only a few parameters. Here we discuss some of these simplifications and their possible effects on the results.

[47] Although these are time-dependent simulations, we have not attempted to truly capture the time-dependent nature of volcanic eruptions. In our simulations, fluid temperature, composition, velocity, pressure and density at the vent are fixed; the highly time-dependent nature of the conduit and magma chamber dynamics is neglected. For example, *Anilkumar et al.* [1993] and *Neri and Gidaspow* [2000] show that large fluctuations in particulate distribution exist in high-speed flows, which would lead to an unsteady vent condition. Our simulations assume a constant particulate distribution in time and space across the vent allowing for the formation of relatively stable shock waves. If the particulate distribution is uneven at the vent exit, this may inhibit the establishment of a Mach stem and the associated velocity profile.

[48] A significant simplification in this study is the use of the pseudogas approximation, which has been applied numerous times in volcanic literature [e.g., *Kieffer and Sturtevant*, 1984; *Woods*, 1988; *Suzuki et al.*, 2005]. One of the main assumptions of the pseudogas approximation is that the entrained solid particles maintain their homogeneous distribution throughout the flow field. In reality, the fluid dynamics of a multiphase mixture interacting in a supersonic compressible flow with shock waves is far more complicated and is not yet fully understood. The pseudogas approximation is capable of representing the fluid dynamics to first order for the purposes of this study. In fact, several other numerical studies of overpressured volcanic jets using multiphase formulations show many of the same features quantified in this study [e.g., *Eposti Ongaro and Neri*, 1999; *Neri et al.*, 2002; *Pelanti*, 2005].

[49] We also have not included gravity or a stratified atmosphere. On the basis of energy balance principles, this is not likely to produce a significant difference in the small and medium jets of this study. However, the presence of gravity and atmospheric stratification may have an small influence on the scale of the shock structure in the kilometer-scale jets. In addition, as the surrounding atmosphere is entrained in the hot eruptive fluid, the plume would become buoyant. Therefore gravity and atmosphere may have an effect on the dynamics of the shear layer downstream of the Mach disk. However, in the gas-thrust region, inertia dominates the flow. It is unlikely that the lack of buoyancy is strongly affecting the results presented here. We show the effects of vent pressure on buoyant jets by *Ogden et al.* [2008].

[50] Spatial resolution is limited in all computational simulations and so there is a question of accuracy. We have tested the sensitivity of our results to doubling the spatial resolution in each direction and have found that the values in Figures 4, 10, 11, and 13 change by less than the errors in the curve approximations.

[51] One of the important aspects of volcanic plume dynamics is the production of turbulent eddies at the jet boundaries. These eddies are necessary for the entrainment and heating of ambient air and are ultimately responsible for the buoyant nature of volcanic plumes. Since this study is primarily concerned with the shock structures in the inertial jet region, we used no subgrid-scale turbulence model. However, the generation of turbulence at the shear layers plays an important role in the stability of the Mach disk. Many of the resolved eddies formed in the turbulent shear layer between our slow moving core and fast moving sheath rapidly spin into the standing Mach disk causing distortions of up to tens of percent of the total Mach disk height. The effects of the unresolved turbulence will be investigated in the future using a subgrid-scale turbulence model.

5. Conclusions

[52] Many explosive volcanic eruptions likely involve overpressured sonic or supersonic vent conditions at some point during their activity. The nature of these eruptions strongly depends on the rapid expansion of the fluid out of the vent and the presence of standing shock structures. Studying this complex flow improves our understanding of the connection between the observed plume profiles and the velocities and pressures at the vent. Using our computational simulations, we quantify the effects of the ratio of vent pressure to atmospheric pressure (K) on large scale overpressured (K > 1) jets as follows.

[53] 1.) Jet decompression in volcanic plumes takes place at minimum up to the height (h_{disk}) of the standing shock wave (the Mach disk), which can be approximated as $h_{disk} = 1.7 r_{vent} K^{1/2}$, where r_{vent} is the vent radius. This is a much larger portion of the plume than is assumed in most other models.

[54] 2.) The radius of the plume (r_{peak}) just above the height of the first Mach disk depends on overpressure and can be estimated by $r_{peak} = r_{vent} K^{1/2}$. This relationship provides a vent pressure estimate that can be made from simple visual and field observations of plume and vent radii.

[55] 3.) The peak vertical heat flux (q_{peak}, Jm^{-2} s^{-1}) in the plume above the Mach disk is drastically reduced by vent overpressure. Relative to the vertical heat flux at the vent (q_{vent}), this effect is quantified by $q_{peak} = 3q_{vent}K^{-5/4}$.

[56] 4.) The presence of standing barrel shocks and Mach disks strongly influences the distribution of vertical heat flux in the lower part of the eruption column. Rather than a Gaussian or top-hat profile that is typically used in plume modeling, our simulations show that the vertical heat flux takes on an *annular* profile in the gas-thrust region after the fluid passes through the standing shock waves. This profile develops because of the decrease in velocity, by two orders of magnitude, in the core of the jet after it passes through the standing Mach disk. Fluid in the outer region of the jet does not pass through a strong shock wave and therefore becomes a fast moving sheath that surrounds the slow moving core. The thickness (w) of this sheath above the first Mach disk can be estimated by $w = \frac{1}{6}r_{vent}K^{3/4}$.

[57] Although these quantifications are robust for the simulations performed here, it is important to keep in mind the limitations of this study. These results are not meant to stand alone as a description of the flow field of any volcanic jet since they lack the time dependent effects of conduit dynamics, a robust treatment of the multiphase dynamics, and consideration of crater effects. These results do show, however, that high vent pressure can drastically alter the heat flux distribution and plume radius in a way that is not predictable from analytical theory and provide a starting place for the incorporation of overpressure effects into 1D models.

Appendix A: Benchmarking of CFDLib

[58] We validate our codes by simulating well-known laboratory experiments. The approach has the advantage over benchmarking against natural eruptions in that we can compare specific measurable quantities related to the shock structures in overpressured jets, which are the focus of our study. We compare CFDLib simulations to laboratory experiments of sonic underexpanded jets using the methods of *Dartevelle* [2006]. We compare the height of the Mach disk measured in these experiments against time-averaged values from our simulations. There are a number of different laboratory experiments of overpressured jets from which to choose. We use that of *Lewis and Carlson* [1964] who fit an empirical curve to their experiments determining the relationship between overpressure ratio (K), Mach disk height (h_{disk}), nozzle diameter (d), Mach number at the nozzle (M_{vent}), and isentropic expansion coefficient (γ): $h_{disk}/d = 0.69\ M_{vent}(\gamma K)^{1/2}$. Figure A1 shows the results from two different laboratory scale simulations (symbols) and the empirical curve of Lewis and Carlson (line). In the simulations plotted as diamonds, we use a two-dimensional cylindrically symmetric mesh with heights ten times that of the Mach disk and 5 times the Mach disk height in radius. The mesh consists of evenly distributed square grid cells with height and widths of 2×10^{-4} m. The simulations plotted as stars are twice the resolution but half the mesh height. For all of our benchmarking simulations, we use air ($\gamma = 1.4$) as the ambient fluid in the box and the jet fluid and set the inflow velocity to be just sonic ($M_{vent} = 1$). We specify the same temperature for the inflow temperature as the ambient fluid.

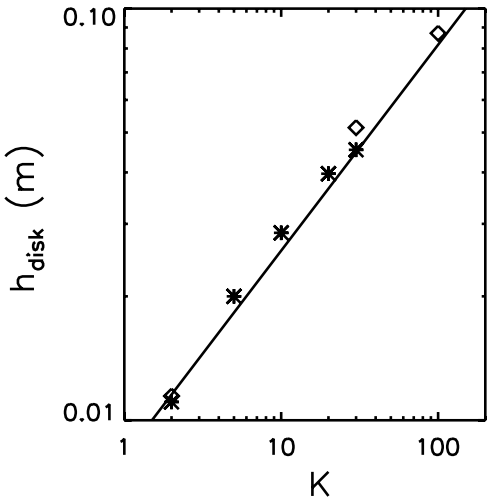

Figure A1. Positive results of benchmark simulations of laboratory underexpanded jets. Simulations based on the laboratory experiments of *Lewis and Carlson* [1964]. Line is a curve fit of the empirical equation determined by Lewis and Carlson. Diamonds are time averaged data from our simulations of air jets at the same scale and inflow velocity. Stars are simulation results at higher resolution but smaller mesh height and width. Diamond simulations have a mesh that is scaled to the Mach disk height in a similar way to the large scale jets of this paper.

[59] To within 10%, the heights of the Mach disk predicted by our simulations match those measured by Lewis & Carlson. In general, our simulations overpredict the Mach disk height slightly. For the purposes of this study, however, we consider the level of this match encouraging as there are many complications to this kind of benchmark. First, it is never possible to exactly simulate a laboratory experiment. For example, our simulations use a flat inflow boundary with a top-hat velocity profile in radius at the vent to represent the nozzle in the experiments. It is unlikely that the fluid in the experiment has a consistent velocity that neglects drag along the nozzle walls. In addition, the exact shape of the nozzle is known to change the height of the first Mach disk [*Addy*, 1981]. Since we are not taking nozzle shape into consideration in these preliminary simulations, some error is introduced here. As with all comparisons to laboratory data, it is important to keep in mind that although simulations afford almost complete spatial and temporal coverage of the system, laboratory data is often dependent on snapshots of often difficult to measure data. In our benchmark, we have chosen to use an empirical formula based on numerous experiments and time averages of our own simulations to help limit the discrepancies that come from comparing snapshots of data.

Notation

c	sound speed (m s^{-1}).
C_P	specific heat capacity of a gas at constant pressure (J kg^{-1} K^{-1}).
C_V	specific heat capacity of a gas at constant volume (J kg^{-1} K^{-1}).
C_S	specific heat capacity of a solid (J kg^{-1} K^{-1}).

h_{disk} Mach disk height (m). Height on jet axis of the standing Mach disk relative to vent exit.

K Overpressure ratio. Ratio of vent pressure (P_{vent}) to atmospheric pressure (P_{atm}).

M Mach number. Ratio of fluid velocity (v) to sound speed in the fluid (c). Subscript: vent- M at the vent, 1- just before the Mach disk, 2- just after the Mach disk.

n Mass fraction volatiles in the pseudogas mixture.

P Pressure (Pa). Subscript: vent- pressure at vent exit, atm- atmospheric pressure and initial pressure in simulation box

q Vertical convective heat flux (J m^{-2} s^{-1}). Subscript: vent- heat flux at the vent, peak-highest heat flux in a horizontal slice located at $z = 1.25h_{disk}$

Q Vertical convective heat flow (J s^{-1}), i.e., heat flux integrated over an area.

r Radius (m), i.e., distance from jet centerline. Subscript: vent- radius of the vent, max- radius of the simulation mesh, peak- horizontal location of q_{peak} relative to jet centerline

R Specific gas constant (J kg^{-1} K^{-1}). Subscript: gas- of the gas portion of the pseudogas, fluid- of the pseudogas itself.

Re Reynolds number. $Re = UL\nu^{-1}$ where L is a characteristic length scale (e.g., the radius of the jet), U a characteristic velocity, and ν the viscous diffusivity of the eruptive fluid.

T Temperature (K). Subscript: vent- at vent, atm- initial temperature in the mesh, fluid-temperature of the eruptive pseudogas

v Velocity (m s^{-1}). Subscript: r- radial component, z- vertical component, vent- at vent (all vertical).

w Approximate thickness of fast moving sheath above the Mach disk (m).

z Vertical distance relative to vent exit (m), i.e., height. Subscript: max- height of computational mesh.

γ Isentropic expansion coefficient for an ideal gas ($\gamma = C_p/C_v$).

Γ Isentropic expansion coefficient for a pseudogas.

ρ Density (kg m^{-3}) Subscript: vent- at the vent.

σ_h Standard deviation of the Mach disk height (h_{disk}) over time.

[60] **Acknowledgments.** Support for this research has been provided by a grant (Astro-1716-07) from the Institute of Geophysics and Planetary Physics, Los Alamos National Laboratory. Computing resources have been provided by an NSF/MRI grant and by a NASA High End Computing allocation. The authors thank Susan Kieffer and Augusto Neri for helpful reviews of this paper.

References

Adamson, T. C., and J. A. Nicholls (1959), On the structure of jets from highly underexpanded nozzles into still air, *J. Aero/Space Sci.*, *26*(1), 16–24.

Addy, A. L. (1981), Effects of axisymmetric sonic nozzle geometry on Mach disk characteristics, *AIAA Journal*, *19*(1), 121–122.

Amsden, A. A., and F. H. Harlow (1968), Numerical calculation of almost incompressible flows, *J. Comput. Phys.*, *3*, 80–93.

Anilkumar, A. V., R. S. J. Sparks, and B. Sturtevant (1993), Geological implications and applications of high-velocity two-phase flow experiments, *J. Volcanol. Geotherm. Res.*, *56*, 145–160.

Antsupov, A. V. (1974), Properties of underexpanded and overexpanded supersonic gas jets, *Soviet Phys. Tech. Phys.*, *19*(2), 234–238.

Chang, I. S., and W. L. Chow (1974), Mach disk from underexpanded axisymmetric nozzle flow, *AIAA Journal*, *12*(8), 1079–1082.

Cheng, T. S., and K. S. Lee (2005), Numerical simulations of underexpanded supersonic jet and free shear layer using WENO schemes, *Int. J. Heat Fluid Flow*, *26*(5), 755–770.

Crist, S., P. M. Sherman, and D. R. Glass (1966), Study of the highly underexpanded sonic jet, *AIAA Journal*, *4*(1), 68–71.

Cumber, P. S., M. Fairweather, S. Falle, and J. R. Giddings (1995), Predictions of the structure of turbulent, highly underexpanded jets, *J. Fluids Eng. Trans. ASME*, *117*(4), 599–604.

Dartevelle, S. (2006), Verification and validation (V&V) methodologies for multiphase turbulent and explosive flows. V&V case studies of computer simulations from Los Alamos National Laboratory GMFIX codes, Abstract V43C-1821, *Eos*, *87*(52).

Dobran, F. (1992), Nonequilibrium-flow in volcanic conduits and application to the eruptions of Mt St-Helens on May 18, 1980, and Vesuvius in AD 79, *J. Volcanol. Geotherm. Res.*, *49*(3–4), 285–311.

Eposti Ongaro, T., and A. Neri (1999), Flow patterns of overpressured volcanic jets, in *European Geophysical Society, XXIV General Assembly*, The Hague.

Ewan, B. C. R., and K. Moodie (1986), Structure and velocity-measurements in underexpanded jets, *Combust. Sci. Tech.*, *45*(5–6), 275–288.

Godunov, S. K. (1999), Reminiscences about difference schemes, *J. Comput. Phys.*, *153*, 6–25.

Gribben, B. J., K. J. Badcock, and B. E. Richards (2000), Numerical study of shock-reflection hysteresis in an underexpanded jet, *AIAA Journal*, *38*(2), 275–283.

Harlow, F. H., and A. A. Amsden (1975), Multifluid flow calculations at all Mach numbers, *J. Comp. Phys.*, *16*, 1–19.

Hishida, K., K. Takemoto, and M. Maeda (1987), Turbulence characteristics of gas-solids two-phase confined jet (effect of particle density), *Japanese J. Multiphase Flow*, *1*, 56–68.

Kashiwa, B. A., and W. B. VanderHeyden (2000), Toward a general theory for multiphase turbulence Part I: Development and gauging of the model equations, in *Los Alamos National Laboratory Report*, pp. 88, Los Alamos National Laboratory, Los Alamos, NM.

Kieffer, S. W. (1977), Sound speed in liquid-gas mixtures - Water-air and water-steam, *J. Geophys. Res.*, *82*(20), 2895–2904.

Kieffer, S. W. (1981), Blast dynamics at Mount St-Helens on 18 May 1980, *Nature*, *291*(5816), 568–570.

Kieffer, S. W. (1982), Fluid dynamics and thermodynamics of Ionian volcanism, in *Satellites of Jupiter*, edited by D. Morrison and M. S. Matthews, University of Arizona Press, Tucson, Ariz.

Kieffer, S. W. (1989), Geologic nozzles, *Rev. Geophys.*, *27*(1), 3–38.

Kieffer, S. W., and B. Sturtevant (1984), Laboratory studies of volcanic jets, *J. Geophys. Res.*, *89*(NB10), 8253–8268.

Ladenburg, R., C. C. Van Voorhis, and J. Winckler (1949), Interferometric studies of faster than sound phenomena. Part II. Analysis of supersonic air jets, *Phys. Rev.*, *76*(5), 662–677.

Legros, F., K. Kelfoun, and J. Marti (2000), The influence of conduit geometry on the dynamics of caldera-forming eruptions, *Earth Planet. Sci. Lett.*, *179*(1), 53–61.

Lewis, C. H. J. R., and D. J. Carlson (1964), Normal shock location in underexpanded gas and gas-particle jets, *AIAA Journal*, *2*(4), 776–777.

Li, Y., A. Kirkpatrick, C. Mitchell, and B. Willson (2004), Characteristic and computational fluid dynamics modeling of high-pressure gas jet injection, *J. Eng. Gas Turbines Power-Trans. ASME*, *126*(1), 192–197.

Liepmann, H. W., and A. Roshko (1957), *Elements of Gasdynamics*, 439 pp., Wiley, New York.

Macedonio, G., F. Dobran, and A. Neri (1994), Erosion processes in volcanic conduits and application to the AD 79 eruption of Vesuvius, *Earth Planet. Sci. Lett.*, *121*(1–2), 137–152.

Mastin, L. G. (2007), A user-friendly one-dimensional model for wet volcanic plumes, *Geochem. Geophys. Geosys.*, *8*.

Morton, B. R., G. Taylor, and J. S. Turner (1956), Turbulent gravitational convection from maintained and instantaneous sources, *Proc. R. Soc. Series A, Mathematical and Physical Sciences*, *234*(1196), 1–23.

Neri, A., and D. Gidaspow (2000), Rise hydrodynamics: Simulation using kinetic theory, *AIChE J.*, *46*(1), 52–67.

Neri, A., P. Papale, and G. Macedonio (1998), The role of magma composition and water content in explosive eruptions: 2. Pyroclastic dispersion dynamics, *J. Volcanol. Geotherm. Res.*, *87*(1–4), 95–115.

Neri, A., A. Di Muro, and R. Rosi (2002), Mass partition during collapsing and transitional columns by using numerical simulations, *J. Volcanol. Geotherm. Res.*, *115*, 1–18.

Neri, A., T. Eposti Ongaro, G. Menconi, M. D. Vitturi, C. Cavazzoni, G. Erbacci, and P. J. Baxter (2007), 4D simulation of explosive eruption dynamics at Vesuvius, *Geophys. Res. Lett.*, *34*(4), L04309, doi:10.1029/2006GL028597.

Norman, M. L., L. Smarr, K. H. A. Winkler, and M. D. Smith (1982), Structure and dynamics of supersonic jets, *Astron. Astrophys.*, *113*(2), 285–302.

Ogden, D. E., G. A. Glatzmaier, and K. H. Wohletz (2008), Effects of vent overpressure on buoyant eruption columns: Implications for plume stability, *Earth Planet. Sci. Lett.*, doi:10.1016/j.epsl.2008.01.014.

Ouellette, P., and P. G. Hill (2000), Turbulent transient gas injections, *J. Fluids Eng. Trans. ASME*, *122*(4), 743–752.

Papale, P., A. Neri, and G. Macedonio (1998), The role of magma composition and water content in explosive eruptions – 1. Conduit ascent dynamics, *J. Volcanol. Geotherm. Res.*, *87*(1–4), 75–93.

Pelanti, M. (2005), Wave propagation algorithms for multicomponent compressible flows with applications to volcanic jets, Doctor of Philosophy thesis, University of Washington, Seattle, Washington.

Post, S., V. Iyer, and J. Abraham (2000), A study of near-field entrainment in gas jets and sprays under diesel conditions, *J. Fluids Eng. Trans. ASME*, *122*(2), 385–395.

Sparks, R. S. J., M. I. Bursik, S. N. Carey, J. S. Gilbert, L. S. Glaze, H. Sigurdsson, and A. W. Woods (1997a), *Volcanic plumes*, xii, 574 pp., Wiley, Chichester; New York.

Sparks, R. S. J., M. C. Gardeweg, E. S. Calder, and S. J. Matthews (1997b), Erosion by pyroclastic flows on Lascar volcano, Chile, *Bull. Volcanol.*, *58*(7), 557–565.

Suzuki, Y. J., T. Koyaguchi, M. Ogawa, and I. Hachisu (2005), A numerical study of turbulent mixing in eruption clouds using a three-dimensional fluid dynamics model, *J. Geophys. Res.*, *110*(B8), B08201, doi:10.1029/2004JB003460.

Thompson, P. A. (1972), *Compressible-Fluid Dynamics*, xvii, 665 pp., McGraw-Hill, New York.

Valentine, G. (1998), Eruption column physics, in *From Magma to Tephra : Modeling Physical Processes of Explosive Volcanic Eruptions*, edited by A. Freundt and M. Rosi, pp. 318, Elsevier, Amsterdam; New York.

Valentine, G. A., and K. R. Groves (1996), Entrainment of country rock during basaltic eruptions of the Lucero volcanic field, New Mexico, *J. Geol.*, *104*(1), 71–90.

Valentine, G. A., and K. H. Wohletz (1989), Numerical-models of Plinian eruption columns and pyroclastic flows, *J. Geophys. Res.*, *94*(B2), 1867–1887.

Wilson, L. (1976), Explosive volcanic eruptions; III, Plinian eruption columns, *Geophys. J. R. Astron. Soc.*, *45*(3), 543–556.

Wilson, L., and S. Self (1980), Volcanic explosion clouds: Density, temperature, and particle content estimates from cloud motion, *J. Geophys. Res.*, *85*(B5), 2567–2572.

Wilson, L., R. S. J. Sparks, T. C. Huang, and N. D. Watkins (1978), Control of volcanic column heights by eruption energetics and dynamics, *J. Geophys. Res.*, *83*(NB4), 1829–1836.

Wohletz, K. H., T. R. McGetchin, M. T. Sandford, and E. M. Jones (1984), Hydrodynamic aspects of caldera-forming eruptions – Numerical-models, *J. Geophys. Res.*, *89*(NB10), 8269–8285.

Wohletz, K. H., D. E. Ogden, and G. A. Glatzmaier (2006), Preliminary numerical simulations of nozzle formation in the host rock of supersonic volcanic jets, Abstract V41C-1748, *Eos*, *87*(52).

Woods, A. W. (1988), The fluid dynamics and thermodynamics of eruption columns, *Bull. Volcanol.*, *50*(3), 169–193.

Woods, A. W. (1995), The dynamics of explosive volcanic-eruptions, *Rev. Geophys.*, *33*(4), 495–530.

Woods, A. W. (1998), Observations and models of volcanic eruption columns, in *The Physics of Explosive Volcanic Eruptions*, edited by J. S. Gilbert and R. S. J. Sparks, pp. 186, Geological Society, London.

Woods, A. W., and S. M. Bower (1995), The decompression of volcanic jets in a crater during explosive volcanic eruptions, *Earth Planet. Sci. Lett.*, *131*(3–4), 189–205.

Wu, P. K., M. Shahnam, K. A. Kirkendall, C. D. Carter, and A. S. Nejad (1999), Expansion and mixing processes of underexpanded supercritical fuel jets injected into superheated conditions, *J. Propulsion Power*, *15*(5), 642–649.

Young, W. S. (1975), Derivation of free-jet Mach-disk location using entropy-balance principle, *Phys. Fluids*, *18*(11), 1421–1425.

Yüceil, K. B., and M. V. Ötügen (2002), Scaling parameters for underexpanded supersonic jets, *Phys. Fluids*, *14*(12), 4206–4215.

E. E. Brodsky, G. A. Glatzmaier, and D. E. Ogden, Earth & Planetary Sciences Department, University of California at Santa Cruz, 1156 High Street, Santa Cruz, CA 95064, USA. (dogden@es.ucsc.edu)

K. H. Wohletz, Los Alamos National Laboratory, EES11 MS F665, Los Alamos, NM 87545, USA.